Bull. Astr. Soc. India (1984) 12, 384–392

Multiple scattering and the dependence of the phase variation of equivalent widths on line profiles

R. K. Bhatia and K. D. Abhyankar
Centre of Advanced Study in Astronomy, Osmania University, Hyderabad 500 007

Received 1984 January 11; accepted 1984 July 5

Abstract. An explanation for the inverse phase effect for absorption lines formed in a Rayleigh scattering atmosphere is given in terms of multiple scattering. It is pointed out that the inverse phase effect is a function of the line profile chosen, with the Lorentz profile giving the maximum change and the Doppler profile the least.

Key words : radiative transfer—line profiles

1. Introduction

The phase variation of equivalent widths in the case of Venus has received considerable theoretical and observational attention (see references in Bhatia & Abhyankar 1981). Comparison of theoretically computed phase curves with observations helps to place constraints on the modelling of the Cytherean atmosphere. Almost all the theoretical studies have taken into account (i) a homogeneous or an inhomogeneous atmosphere, and (ii) different phase functions to represent the angular dependence of scattering. No study seems to have been made of the effect of the shape of the absorption line profile on the phase curve, most of the authors having chosen to represent the absorption by a Lorentz profile.

As pointed out below, the region in the atmosphere where bands originate has not been unambiguously identified. Consequently, it is of interest to see the dependence of the phase effect on the line profile, which is quite distinct from the curve-of-growth effect. In this paper we study this dependence for three line profiles in the integrated light of the planet whose atmosphere, for simplicity, is supposed to be semi-infinite, plane parallel and homogeneous. By homogeneous we mean an isobaric and isothermal atmosphere with a constant ratio of scattering to absorption. The scattering in the atmosphere is represented by Rayleigh's phase matrix which is realistic for scattering by molecules. The scattering diagrams for the two components and also for the total intensity are shown in figure 1. Here we shall compare the variations in the case of the Lorentz profile with those for a Doppler profile and a Voigt profile. Some of the considerations which have prompted us to take up this study are as follows.

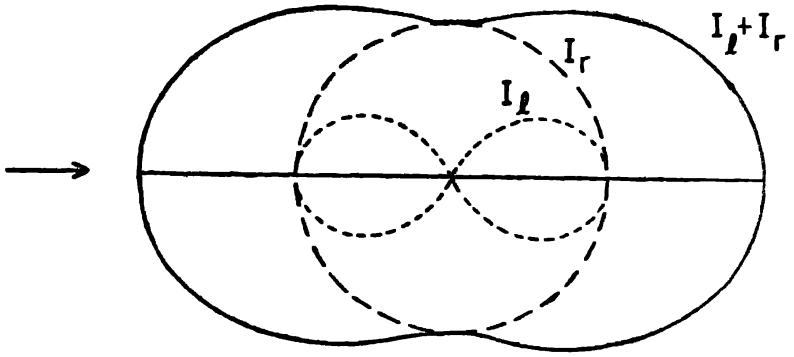

Figure 1. Scattering diagrams for Rayleigh scattering for the Stokes components I_l, I_r and for the total intensity $I = I_l + I_r$.

(i) Multiple scattering is a complex process even under the simplest conditions. To gain physical insight into this complex process, it is imperative that initially a simple atmosphere be used; multiple scattering studies in an inhomogeneous atmosphere can follow after we have a fair idea of what happens under simple conditions. This will save a lot of computational effort because multiple scattering is the basis of all the information inferred about planetary atmospheres; it is the common factor, whatever be the assumed structure of the atmosphere. For example, to the best of our knowledge, no detailed explanation has been given as to why certain phase functions give the inverse phase effect although Whitehill & Hansen (1973) and Young & Kattawar (1977) did comment on the role of the shape of the phase function.

(ii) The exact location where the absorption bands originate in the atmosphere has not been satisfactorily deduced. Young *et al.*'s (1980) observations indicate that the Mie-scattering model, which explains so well the phase variation of continuum polarization, does not explain the phase variation of equivalent widths. Bhatia & Abhyankar (1982) have argued that a two-layer model in which a Rayleigh scattering layer (where the lines are formed) overlies a Mie-scattering deck (where the continuum polarization originates) can explain both the variations. Mukai & Mukai (1981) and Santer & Dollfus (1980) have postulated from independent considerations the existence of sub-micron size particles high in the atmosphere of Venus, thereby lending credence to the hypothesis that the lines originate in a Rayleigh-scattering region. Further, Young (1977) noted the correlation of the change in the $(U - V)$ colour with that of the equivalent widths. Therefore, it is likely that bands are formed in a region of low pressure (Doppler profile domain) in a Rayleigh-scattering region. Note that Young (1977) had pointed out that the resolving power of existing instrumentation ($\sim 3 \times 10^5$) is not sufficient to resolve the Doppler core, the required power being 1.5×10^6. However, the effect of the Doppler core will definitely show up in equivalent width measurements; consequently, computations for a Doppler profile do have meaning.

(iii) It is to be noted that Kattawar & Young (1977) found that the shape of the phase curve is not very sensitive to pressure and temperature variations in the atmosphere; only the absolute equivalent widths change. Since here we are concerned only with the shape of the phase curve, the assumption of a homogeneous

atmosphere seems satisfactory. However, it should be emphasized that we are not arguing that the atmosphere of Venus is homogeneous.

3. Basic theory

3.1. *Radiative transfer*

Let unpolarized radiation of flux $\pi\mathcal{F}$, having the components $\pi\mathcal{F}_l$ and $\pi\mathcal{F}_r$ be incident on a plane-parallel atmosphere in the direction $(-\mu_0 = \cos\theta_0, \varphi_0)$. Here l and r denote directions parallel and perpendicular to the meridian plane defined by the incident ray. Then, the three components I_l, I_r and U of the scattered radiation I in the direction (μ, φ), where l and r are now directions parallel and perpendicular to the meridian plane defined by the scattered ray, are given by (Chandrasekhar 1960; Bhatia & Abhyankar 1982)

$$I_l(\mu, \varphi) = \frac{3}{32}\frac{\mu_0\varpi_0}{\mu + \mu_0}[L_1(\mu)[L_1(\mu_0) + L_3(\mu_0)] + L_2(\mu)[L_2(\mu_0) + L_4(\mu_0)] - 4\mu\mu_0(1-\mu^2)^{1/2}(1-\mu_0^2)^{1/2} H^{(1)}(\mu) \times H^{(1)}(\mu_0)\cos(\varphi_0 - \varphi) + \mu^2(\mu_0^2 - 1) H^{(2)}(\mu) H^{(2)}(\mu_0) \times \cos 2(\varphi_0 - \varphi)]\mathcal{F}, \quad \ldots(1)$$

$$I_r(\mu, \varphi) = \frac{3}{32}\frac{\mu_0\varpi_0}{\mu + \mu_0}[L_3(\mu)[L_1(\mu_0) + L_3(\mu_0)] + L_4(\mu)[L_2(\mu_0) + L_4(\mu_0)] - (\mu_0^2 - 1) \times H^{(2)}(\mu) H^{(2)}(\mu_0)\cos 2(\varphi_0 - \varphi)]\mathcal{F}, \quad \ldots(2)$$

$$U(\mu, \varphi) = \frac{3}{32}\frac{\mu_0\varpi_0}{\mu + \mu_0}[2\mu_0(1-\mu^2)^{1/2}(1-\mu_0^2)^{1/2} \times \sin(\varphi_0 - \varphi) H^{(1)}(\mu_0)\mu(\mu_0^2 - 1) \times \sin 2(\varphi_0 - \varphi) H^{(2)}(\mu) H^{(2)}(\mu_0)]\mathcal{F}. \quad \ldots(3)$$

$I = I_l + I_r$ gives the total intensity. Here ϖ_0 is the single scattering albedo, and the necessary functions have been tabulated by Abhyankar & Fymat (1971). Further, it is assumed that no frequency redistribution takes place.

3.2. *Computation of integrated flux*

After applying the necessary transformations equations (*cf.* Bhatia & Abhyankar 1982) to the Stokes parameters of the scattered radiation to refer them to a common coordinate system with intensity components parallel and perpendicular to the intensity equator of the planet, we use Horak's (1950) method for obtaining the fluxes F_l^e, F_r^e and $F = F_l^e + F_r^e$ integrated over the visible disc. Here F_l^e is the vector component which vibrates parallel, and F_r^e perpendicular to the intensity equator.

3.3. *Line profile*

The variation of absorption with frequency along a line, the absorption line profile, is

$$k_\nu = k_0 X.$$

There k_0 is the absorption at the line centre and X gives the variation of k_ν and is a function of the type of line profile. X can take three (or more) forms :

$$X = (1 + x^2)^{-1} \quad \text{(Lorentz)}$$

$$X = H(a, x) \quad \text{(Voigt)}$$

$$X = e^{-x^2} \quad \text{(Doppler)}$$

Here x is the distance from the line centre in units of the half-width. For the Lorentz profile, $x = (\nu - \nu_0)/\alpha_L$, ($\alpha_L$ = Lorentz half-width) and for the Voigt and Doppler profiles $x = (\nu - \nu_0)/\alpha_D$, ($\sqrt{\ln 2}\alpha_D$ = Doppler half-width). For the Voigt profile, $a = \alpha_L/\alpha_D$ gives the relative importance of pressure broadening to that of Doppler broadening. The functions $H(a, x)$ have been tabulated by Finn & Muggle-stone (1965). Note that the Lorentz profile ($a = \infty$) has the maximum extent of wings, the Doppler profile ($a = 0$) the least and the Voigt profile somewhere between the two, depending on the value of a.

The absorption coefficient is related to the single scattering albedo through

$$\varpi_\nu = \frac{\sigma}{\sigma + k_\nu + k_c},$$

where σ is the scattering coefficient, k_ν the line absorption coefficient and k_c the continuum absorption coefficient. A little algebra leads to

$$\varpi_\nu = \left[\left(\frac{1 - \varpi_0}{\varpi_0}\right) X + \frac{1}{\varpi_c}\right]^{-1}, \qquad \ldots(5)$$

where ϖ_0 is the absorption coefficient at the line centre without continuum absorption and ϖ_c is the continuum scattering albedo inferred from Bond albedo measurements.

Comparison of phase curves for the three profiles requires that we compare lines of equal strength. To do so, let us first set the Doppler half-width equal to the Lorentz half-width *i.e.*, $\alpha_L = \sqrt{\ln 2}\alpha_D$. Since $S/\sigma = k_0^L \pi\alpha_L$ for the Lorentz profile and $S/\sigma = (k_0^D \sqrt{\pi}\, \alpha_D)/\sigma$ for the Doppler and Voigt profiles (S being the line intensity) for the same strength of the line we have $k_0^D = k_0^L \sqrt{\pi \ln 2}$, which gives

$$\left(\frac{1}{\varpi_0^D} - 1\right) = 1.47566 \left(\frac{1}{\varpi_0^L} - 1\right). \qquad \ldots(6)$$

The equivalent width is defined by

$$W = \int_{\text{line}} \left(1 - \frac{F_\nu}{F_c}\right) d\nu, \qquad \ldots(7)$$

where F_ν is the flux at any frequency and F_c the continuum flux. We can similarly define equivalent widths for the two Stokes components F_l^e and F_r^e separately.

Using equations (1)–(3) and after integrating over the visible disc, we have computed the emergent fluxes for different phase angles α. Further, using equations (5)–(7) we have computed the equivalent widths for the three profiles for three

different line strengths corresponding to $\varpi_0^L = 0.1$ (very strong line), 0.9 (weak line) and 0.9999 (very weak line) taking $\varpi_c = 0.99$ in all three cases. These results are discussed below.

4. Results and discussion

The phase variation of the relative equivalent widths for the three lines (strong, weak and very weak), normalized to the value at $\alpha = 0$, are shown in figures 2–4 for the Lorentz, Voigt and Doppler profiles. An inspection of these figures shows that : (i) the inverse phase effect is exhibited by all the profiles for the F_l^e component and for the total flux F; the F_r^e component shows the familiar normal phase effect (with a very small inverse phase effect between $0 < \alpha < 40$); and (ii) the phase effect is an inverse function of the line strength. We now discuss these results in detail.

4.1. An explanation for the inverse phase effect in terms of multiple scattering

Let us consider $W(\alpha)/W(0)$, $W(\alpha)$ being the equivalent width at any phase angle α and $W(0)$ the equivalent width at phase angle 0. Now, for the inverse phase effect

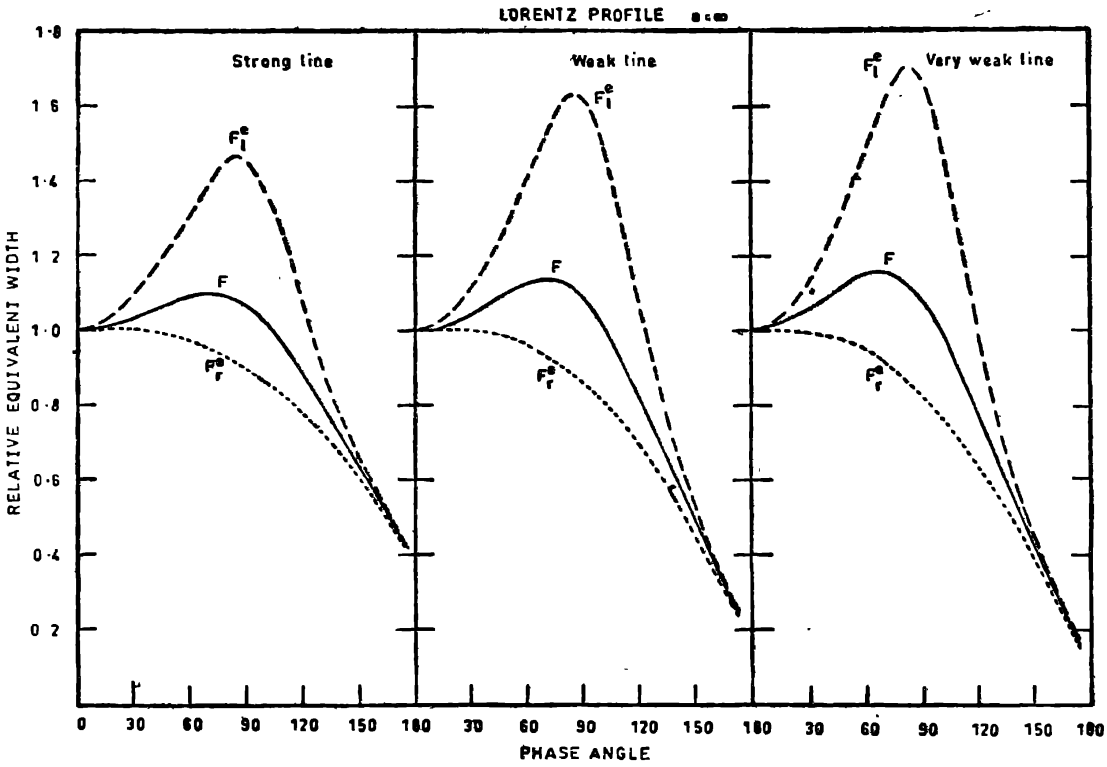

Figure 2. Variation of the relative equivalent width with phase angle for the F_l^e, F_r^e components and total flux $F = F_l^e + F_r^e$ for the Lorentz profile ($a = \infty$) for three line strengths corresponding to $\varpi_0^L = 0.1$, 0.9 and 0.9999.

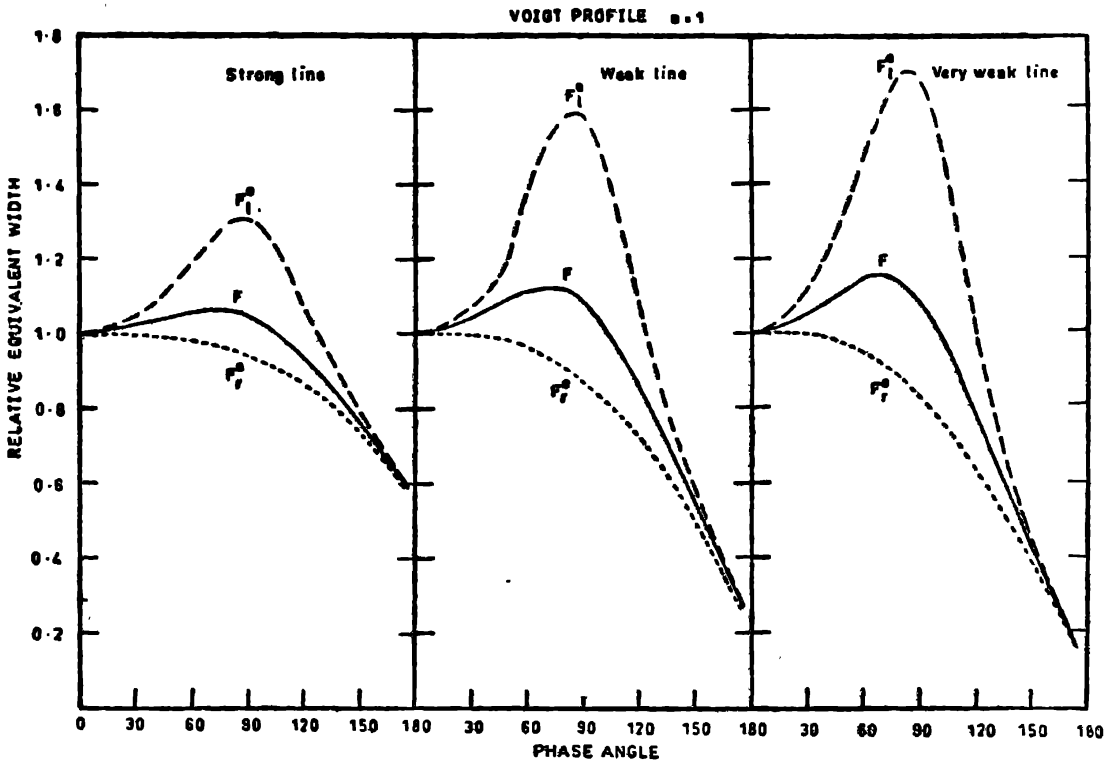

Figure 3. Same as figure 2 but for the Voigt Profile ($a = 1$)

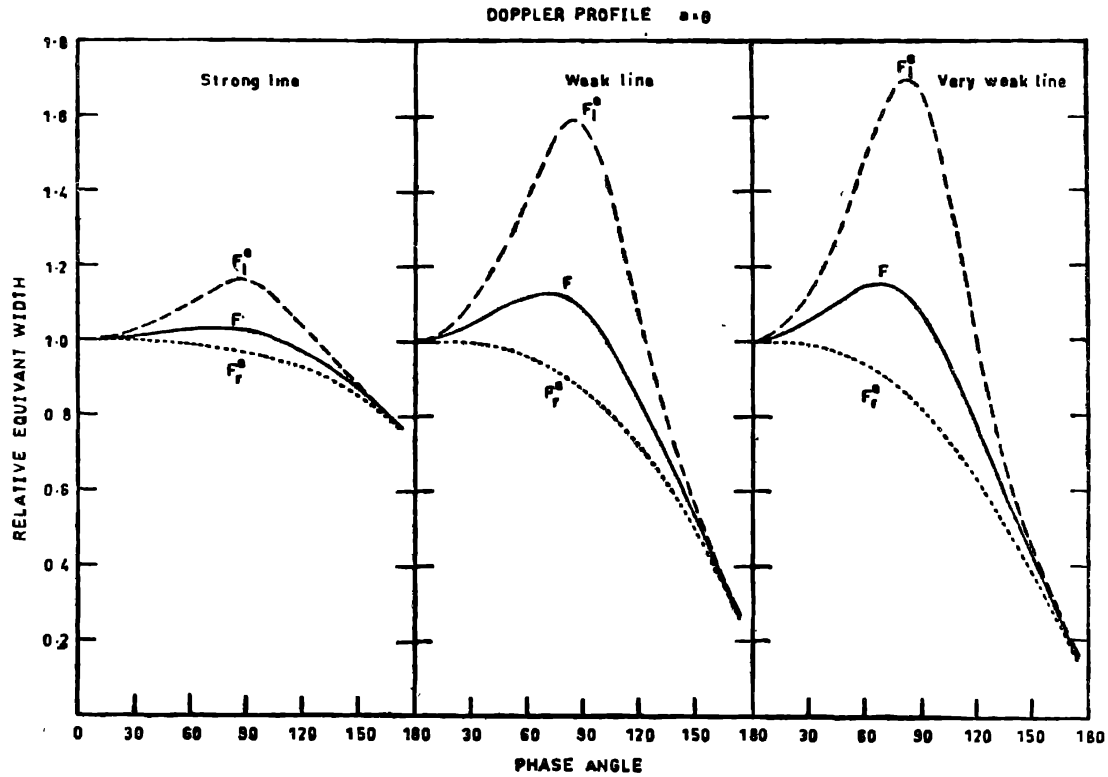

Figure 4. Same as figure 2 but for the Doppler Profile ($a = 0$)

to appear, $W(\alpha)$ must increase with increasing phase angle (say up to $\alpha = 90$). From the definition of the equivalent width we see that for an increased equivalent width at any phase angle α, we require that the rate of change of flux should increase (compared with that at $\alpha = 0$) as we go from the line centre outwards. Let us now see how the flux changes for three different values of the albedo (0.1, 0.9 and 0.997), noting that the albedo and frequency are related by equation (5).

Table 1 gives the flux ratios for F_l^e, F_r^e and F in terms of those at $\alpha = 0$. Since we are dealing with a symmetric phase function, we shall confine our discussions to the phase angle and not the scattering angle. Referring to figure 1, we see that the phase function for F_l decreases as α increases, reaches zero at $\alpha = 90$ and then increases again with increasing α. How does the flux ratio change for different albedos ? We note from table 1 that the flux ratio drops the fastest for $\varpi_0 = 0.1$ and the slowest for $\varpi_0 = 0.997$. In other words, the ratio F_v/F_c decreases with phase angle from the line centre outwards leading to an increase in equivalent width. Why does the rate of change differ for different albedos ? This is so because the photons have random walked in the atmosphere before emerging.

Table 1. Change in the relative fluxes with phase angle α for F_l^e, F_r^e and for three albedos $\varpi_0 = 0.1$, 0.9 and 0.997.

	F_l^e			F_r^e			F		
$\alpha \backslash \varpi$	0.1	0.9	0.997	0.1	0.9	0.997	0.1	0.9	0.997
0	1.000	1.000	1.000	1.000	1.000	1.000	1.000	1.000	1.000
20	.818	.852	.878	.926	.932	.934	.872	.892	.906
40	.463	.550	.620	.783	.785	.786	.622	.668	.701
60	.160	.278	.367	.618	.607	.593	.389	.442	.480
80	.019	.126	.199	.453	.428	.403	.236	.277	.301
90	.004	.117	.148	.375	.382	.317	.190	.249	.233
100	.013	.073	.113	.301	.268	.240	.157	.173	.177
120	.045	.065	.069	.174	.142	.119	.110	.103	.094
135	.050	.048	.042	.099	.074	.058	.074	.061	.051
150	.033	.025	.019	.044	.030	.022	.034	.027	.021
175	.001	.0006	.0004	.001	.0005	.000	.000	.0006	.000

α is the phase angle

Let us suppose that the photons emerge after n collisions; then, the angle between the directions defining the nth and $(n - 1)$th collisions will be different for different photons. Equivalently, there will be a random superpositioning of the same scattering diagram. This is what gives rise to the unequal rate of change of flux for different albedos; for $\varpi_0 = 0.1$ the ratio decreases till $\alpha = 90$ and then increases again till $\alpha = 135$ (despite the fact that the size of the planetary disc is continuously decreasing) before decreasing again as α increases further; note how the change of ratio follows the scattering diagram. However, for $\varpi_0 = 0.9$ and $\varpi_0 = 0.997$, defining photons which are characterized by a large number of scatterings, there is a continuous decrease with increasing phase angle. This is due to the fact that the dip in the phase function at $\alpha = 90$ is filled out due to the random superpositioning of the scattering diagram. This can also explain why the inverse phase effect is more for the F_l^e component than for the total flux F. It is because

of the sharper drop for the former in the value of the phase function at $\alpha = 90$. The F_r^e component on the other hand shows a very small inverse phase effect between $\alpha = 0$ and 40 but otherwise gives the normal phase effect as it should because it is almost isotropically scattered. Indeed, we have established elsewhere (Bhatia & Abhyankar 1983) that any phase function having a dip in the range $0 < \alpha < 180$ will show the inverse phase effect and that it is not due to a backward scattering lobe; only the peaking of the inverse phase effect depends on the position of the dip.

4.2. Dependence of phase effect on line profile and line strength

Let us now try to understand why the Lorentz profile gives an enhanced inverse phase effect compared to the other two profiles. Owing to multiple scattering effects, the photons entering a scattering atmosphere will random walk in the atmosphere. Consequently, the emergent photons characterizing a particular albedo will have originated at different depths in the atmosphere. This brings us to the question: can an average optical depth be assigned to each value of ϖ, and consequently to different parts of the line (*cf.* equation (5))? This idea was introduced by Chamberlain (1965), who also estimated the value of $\langle\tau\rangle$. Abhyankar and Bhatia (1983) arrived at another estimate of $\langle\tau\rangle$ using a different approach which incorporated the complete dependence on the geometry as also on ϖ. Their analysis shows that $\langle\tau\rangle$ increases with increasing ϖ, which is valid on physical grounds: a larger value of ϖ implies smaller absorption, leading to a deeper penetration of the photon into the atmosphere. This gives rise to a larger value of $\langle\tau\rangle$.

We know that ϖ increases from the line centre outwards (*cf.* equation (5)). We therefore see that $\langle\tau\rangle$ is small for the centre of the line and increases towards the wings. We can define an effective $\langle\tau\rangle_l$ for the whole line (this, in effect, is a second order averaging)

$$\langle\tau\rangle_l = \int_{\text{line}} \langle\tau\rangle_\nu \left(1 - \frac{F_\nu}{F_c}\right) d\nu \Big/ \int_{\text{line}} \left(1 - \frac{F_\nu}{F_c}\right) d\nu. \qquad \ldots(8)$$

Here $\langle\tau\rangle_\nu$ is the effective depth at any frequency ν on the line. We know that the Lorentz profile has the maximum extent of the wings and the Doppler profile the least. It follows from the above definition of $\langle\tau\rangle_l$ that $\langle\tau\rangle_l$ (Lorentz) $>$ $\langle\tau\rangle_l$ (Voigt) $>$ $\langle\tau\rangle_l$ (Doppler). This implies that an absorption line (taken as a whole) represented by a Lorentz profile is formed deeper in the atmosphere compared with the other two profiles. This would be true at any phase angle.

It is evident that as a planet moves away from phase angle 0, the effective optical depth at which lines are formed moves upwards in the atmosphere; therefore $\langle\tau\rangle_l$ will decrease. Evidently, the rate at which this effective depth moves upwards in the atmosphere with changing phase angle will be maximum for the Lorentz profile and the least for the Doppler profile. Since the relative change in equivalent width is proportional to the change in the effective optical depth, absorption lines for the Lorentz profile will show the maximum change and that for the Doppler profile the least.

An extension of the above argument also explains why weaker lines show more change compared to stronger lines (for the same line profile). The effective depth for the weaker line is more compared to that for the stronger line (*cf.* equation (8)).

Again, as the planet moves away from phase angle 0, the change in effective optical depth will be more for the weaker line, leading to a larger relative change in equivalent width.

5. Conclusions

We have pointed out that we do not have sufficiently strong reasons to believe that the Lorentz profile is the best profile for representing absorption line fomation in the Venus atmosphere. There is a distinct possibility that a Voigt profile would be the best representation. We have shown that as the contribution from the wings drops, the phase curves become flatter since strong lines are formed high in the atmosphere and the weaker lines deeper (*e.g.* Young 1969, Abhyankar & Bhatia 1983). We shall have to consider the possibility of using different profiles for lines of different strength. Further, at large phase angles almost all the bands are formed in the upper layers of the atmosphere. Consequently, different profiles may have to be used in the ranges $0 < \alpha < 100$ and $100 < \alpha < 180$.

References

Abhyankar, K. D. & Fymat, A. L. (1971) *Ap. J. Suppl.* **23**, 35.
Abhyankar, K. D. & Bhatia, R. K. (1984) *Earth, Moon, Planets* **30**, 175.
Bhatia, R. K. & Abhyankar, K. D. (1981) *Bull. Astr. Soc. India* **9**, 181.
Bhatia, R. K. & Abhyankar, K. D. (1982, 1983) *J. Astr. Ap.* **3**, 303; *Ap. Sp. Sci.* **96**, 107.
Chandrasekhar, S. (1960) *Radiative Transfer*, Dover.
Finn, G. D. & Mugglestone, D. (1965) *M.N.R.A.S.* **129**, 221.
Horak, H. G. (1950) *Ap. J.* **112**, 445.
Kattawar, G. W. & Young, L. D. G. (1977) *Icarus* **30**, 179.
Lestrade, J. P. & Chamberlain, J. W. (1980) *Icarus* **44**, 813.
Mukai, S. & Mukai, T. (1981) *Icarus* **48**, 482.
Santer, R. & Dollfus, A. (1980) *Astr. J.* **85**, 751.
Whitehill, L. P. & Hansen J. E (1973) *Icarus* **20**, 146.
Young, A. T. (1977) *Icarus* **32**, 1.
Young, L. D. G. (1970) *Icarus* **13**, 449.
Young, L. D. G. & Kattawar, G. W. (1977) *Icarus* **30**, 360.
Young L. D, G., Schorn, R. A. J. & Young, A. T. (1980) *Icarus* **41**, 309.